ELSEVIER

Ceramics International 29 (2003) 213–221

CERAMICS INTERNATIONAL

www.elsevier.com/locate/ceramint

Sliding wear and fracture mechanisms of injection molded Cr_3C_2/Al_2O_3 composite

Ching-An Jeng[a], Jow-Lay Huang[a,*], Jen-Fin Lin[b]

[a]*Department of Material Science & Engineering, National Cheng-Kung University, Tainan 701, Taiwan, ROC*
[b]*Department of Mechanical Engineering, National Cheng-Kung University, Tainan 701, Taiwan, ROC*

Received 24 January 2002; received in revised form 5 February 2002; accepted 10 May 2002

Abstract

The wear resistance and fracture mechanisms of Cr_3C_2/Al_2O_3 composites were investigated with a pin-on-disk test configuration against a silicon carbide sphere at room temperature in unlubricated sliding. The results suggest that the microcracking induced from residual stresses could play an important role in predicting the wear behavior. Although the addition of Cr_3C_2 to Al_2O_3 matrix improved its crack growth resistance, it enhanced the wear resistance. The mechanisms of material removal was related to the failure of the particle-matrix interface, resulting in particle pullout, wear debris and chipping of the matrix. A microabrasive mechanism and microplastic deformation were also observed. The worn-induced surface residual stress (−142 MPa) was similar to that induced by no. 270 diamond wheel grinding (−158 MPa).

Keywords: A. Injection molding; B. Composites; C. Wear resistance; Residual stress

1. Introduction

Ceramic matrix composites have been attracted much attention in advanced structural and tribological applications for several decades. Chromium carbide has been used as a potential material for toughening of alumina because of its high Young's modulus and erosion resistance [1]. The promising mechanical properties and high temperature oxidation resistance of Cr_3C_2/Al_2O_3 composites have been reported by many authors [2–6].

The tribological behaviors of some monolithic and transformation toughening ceramic materials were also studied [7–9]. More recently, many of the studies focused on whisker or fiber-reinforced ceramics [10,11]. The mechanism of sliding wear resistance in non-transformable particulate reinforced ceramics is not well understood. In addition, the effects of reinforcing particulates on the R-curve behaviors and the wear properties of ceramic matrix are still in discrepancy [12]. With wear and fracture processes usually occurring on a micro-scale, these conflicting results demonstrate the need for a better understanding of how wear resistance correlates with microstructural properties.

TiC/Al_2O_3 composite has been used as a magnetic head slider due to its good wear resistance and mechanical strength. One major goal of this study is to evaluate the feasibility of using Cr_3C_2/Al_2O_3 composite as a new candidate of slider material. The tribological characteristics and fracture mechanism of Cr_3C_2/Al_2O_3 composite under dry sliding contact were investigated. X-Ray Diffractometers (XRD) were used to study the damage mechanism and surface residual stress at worn track. The injection moulding technique was used for fabricating Cr_3C_2/Al_2O_3 samples in this study because it can produce complex-shaped components with high-dimensional accuracy and has a potential for automatic production.

2. Experimental procedure

2.1. Material preparation

Alumina powders (A16-SG, Alcoa, USA 0.5 μm) were mixed with Cr_3C_2 [2 μm, grade 160, H.C. Stark, Goslar, Germany (10 vol.%)] in a polyurethane bottle with high purity alumina balls and ethanol for 24 h. The

* Corresponding author. Fax: +886-6-2763586.
E-mail address: jlh888@mail.ncku.edu.tw (J.-L. Huang).

0272-8842/03/$22.00
PII: S0272-8842(02)00108-6

slurry was dried in a rotating vacuum evaporator for 20 min. Dried agglomerates were pulverized with an alumina mortar and pestle, and screened through a 100 mesh screen for pulverizing aggregates.

The above powder was milled in a sigma blender (Irie Shokai Co., Japan, PN-1H) for 40 min, and then mixed with binder for another 40 min. The temperature of the mixer was maintained at 200 °C by hot circulating oil. The binder was composed of polypropylene (UBE Indu., Ltd, Japan), paraffin wax (Fluka, Japan) and stearic acid (Katayama, Japan) with a ratio of 30:65:5 by mass.

Green compacts with dimensions of 65×6.1×5.1 mm and 41 mm (diameter) × 5.1 mm were molded using a reciprocating screw injection molding machine (Chen Hsong Machinery Taiwan Co., Ltd., SM-50) under a pressure of 70 MPa, with a holding time of 8 s and injecting velocity of 40 cm^3/s. The barrel temperatures used for injection were 150, 155, 160, 165 °C from feeder to nozzle, separately.

Test samples were soaked in heptane at 40 °C for 5 h, dried in ambient air, and thermally debinded. Samples were then cold isostatically pressed at 100 MPa and sintered in a graphite furnace at 1550 °C for 2 h under vacuum. They were then ground, lapped (GC no. 600) and polished to 1 μm finish.

2.2. Characterization of physical and mechanical properties

The density was measured by the Archimedes method. The hardness was determined by a microhardness indenter (Vickers, Hv. Akashi AVK-A, Japan). The elastic modulus and Poisson's ratio were evaluated from pulse echo method (pulse generator, model 5072, Panametrics, USA and oscilloscope, TDS540C, Tektronix, USA). The thermal expansion coefficients were measured by a dilatometry system designed by the authors.

Flexural strength was measured by the four-point bending test on a universal testing instrument (Series 8562, Instron Corporation, Canton, MA, USA) at a displacement of 0.5 mm/min. The outer and inner spans were 40 and 20 mm, respectively. Test samples were machined into bars with dimensions of 4×5×50 mm with 45° edge chamfers in advance.

2.3. Wear test

Wear tests were carried out in air using a tribometer with a pin-on-disk configuration. A 10 mm (diameter) silicon carbide sphere was used as the pin. Disk samples were machined with dimensions of 38 mm (diameter) × 4.4 mm. Some physical and mechanical parameters of the pin and disk are listed in Table 1. To establish the conditions for a given wear test, a load was placed on the pin at a predetermined location to achieve a desired contact load (98–196 N). The sliding velocity was varied in the range of 0.061–0.245 m/s using a direct-current motor control dial. The whole sliding distance was controlled to 1 km.

Table 1
Some mechanical properties of SiC ball and 10% Cr_3C_2/Al_2O_3 composite

Properties	SiC Ball[a]	10% Cr_3C_2/Al_2O_3 composite
Density (g/cm^3)	3.1	4.15
Grain size (μm)	NA	3–4
Hardness (kg/mm^2)	2500	1700
RT flexural strength (MPa)	493	490
Youngs' modulus (GPa)	394	360
Poisson ratio (−)	0.16	0.24
Melting point (°C)	~2800	3100

[a] The information of SiC ball was supplied by Nippon Kagaku Togyo Co., Ltd, Japan.

The specific wear rate was estimated by the weight difference before and after the wear test with an accuracy of 10^{-4} g. The friction coefficient was calculated from the torque with the following expression

$$\mu = M/(r/F) \quad (1)$$

where M is the torque, r is the radius of the wear track and F is the applied force. Grinding experiments were performed using a resin-bonded 270 grit peripheral diamond wheel (200 mm diameter) with the width of 15 mm. The wheel was dressed with an alumina dressing stick before grinding and a soluble-oil grinding fluid was used for cooling. The wheel surface speed was 20.944 m/s and the table speed was fixed at 0.218 m/s. The depth of grinding was 2 μm/pass and five passes were made to establish a steady-state condition. The specimens (4×25×25 mm) were ground on the 25×25 mm surface.

2.4. Microstructural analysis and stress measurement

The microstructures and the worn surfaces were examined using optical microscopy, scanning electron microscopy (SEM, Hitachi S-2700, Japan), and transmission electron microscopy (TEM, JEOL 3010, Japan). The phases both in sintered and worn samples were analyzed by ESCA (VG Scientific 210XPS, UK) and X-ray diffractometer (Rigaku D/Max-IIB, Japan) using a Cu target and Ni filter with a scanning speed of 4° /min from 20 to 80°. The surface residual stress was measured on a diffractometer (Siemens D-5000, Germany) according to the $\sin^2\psi$ method of Cohen et al. [13,14].

3. Results and discussion

3.1. Friction, wear and fracture

Fig. 1 shows the variations in friction coefficients of monolithic alumina and Cr_3C_2/Al_2O_3 composites with

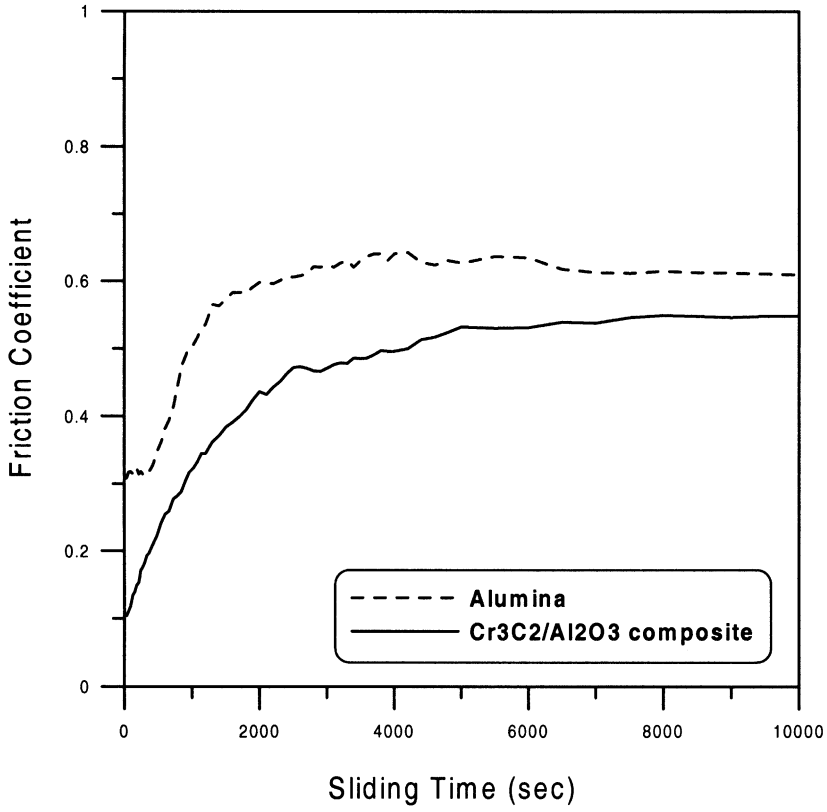

Fig. 1. Friction coefficient evolution as a function of sliding time at 98 N load with line velocity of 0.061 m/s.

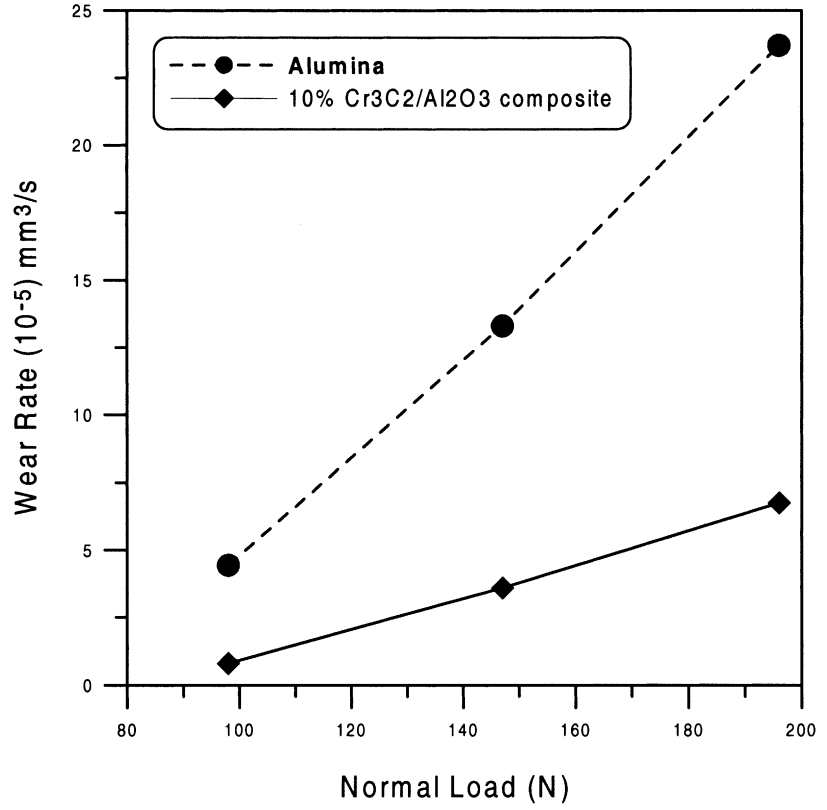

Fig. 2. Volumetric wear rate versus applied load at a sliding speed of 0.245 m/s.

sliding time (wear track length) at the normal load of 98 N and the sliding speed of 0.061 m/s. The friction coefficients for both materials rise slowly until the stationary states are reached. In addition, the friction coefficient of monolithic alumina is consistently greater than that of Cr_3C_2/Al_2O_3 composites. The running-in process is usually associated with the change in surface roughness and the generation of wear debris at the sliding-contact interface.

In Fig. 2, the volumetric wear rates of monolithic alumina and Cr_3C_2/Al_2O_3 composites are plotted versus normal load at a fixed velocity of 0.245 m/s. The specific wear rates for both samples in this configuration were in the range of mild wear regime [15] and followed almost a linear increase with the normal load. The wear rate of Cr_3C_2/Al_2O_3 composites increased moderately, and was consistently lower than that of the monolithic alumina by a factor of about 4.

Fig. 3 shows the wear rates of monolithic alumina and Cr_3C_2/Al_2O_3 composites as a function of line velocity under a constant load of 98 N. The wear rate of Cr_3C_2/Al_2O_3 composites was slightly lower than that of monolithic alumina. At the contact surface, the higher sliding velocity could initiate thermal stresses and intensify thermal cracking [16–18]. Increased load and velocity could increase the number of contact points and generate frictional energy between asperities of the mating surfaces [17]. According to the flash temperature maps calculated by Kong and Ashby [18], the surface temperature may be about 300–400 °C. The combined effects of increased normal load and sliding velocity result in a transition from mild to severe wear due to the interaction of tensile stresses.

In a sliding contact, the surface is subjected to a set of normal and tangential stresses which produce deformation and cause fracture of the material [15]. If the material does not contain evident microcracks, the fracture is controlled by the initiation of microcracks. If microcracks or flaws exist, the fracture process is controlled by the propagation of these microcracks. Spontaneous microcracking induced during the cooling process of sintering has been observed in polycrystalline ceramics with the grain size exceeding a critical value **d** [19]. This is attributed to misfit strains, resulting from thermal expansion anisotropy in single-phase ceramics or thermal expansion mismatch between the matrix and chromium carbide, as shown in Fig. 4. Based on the stored elastic energy converting to the work of fracture in materials, the conditions for spontaneous microcracking have been analyzed by some investigators for a wide variety of reinforcement particle geometries in terms of **d** [19,20], the critical size of reinforcement particles above which microcracking proceeds. **d** is estimated by

$$\boldsymbol{d} = (\Psi\gamma_f)/\left[E_m(\Delta\alpha\Delta T)^2\right] \quad (2)$$

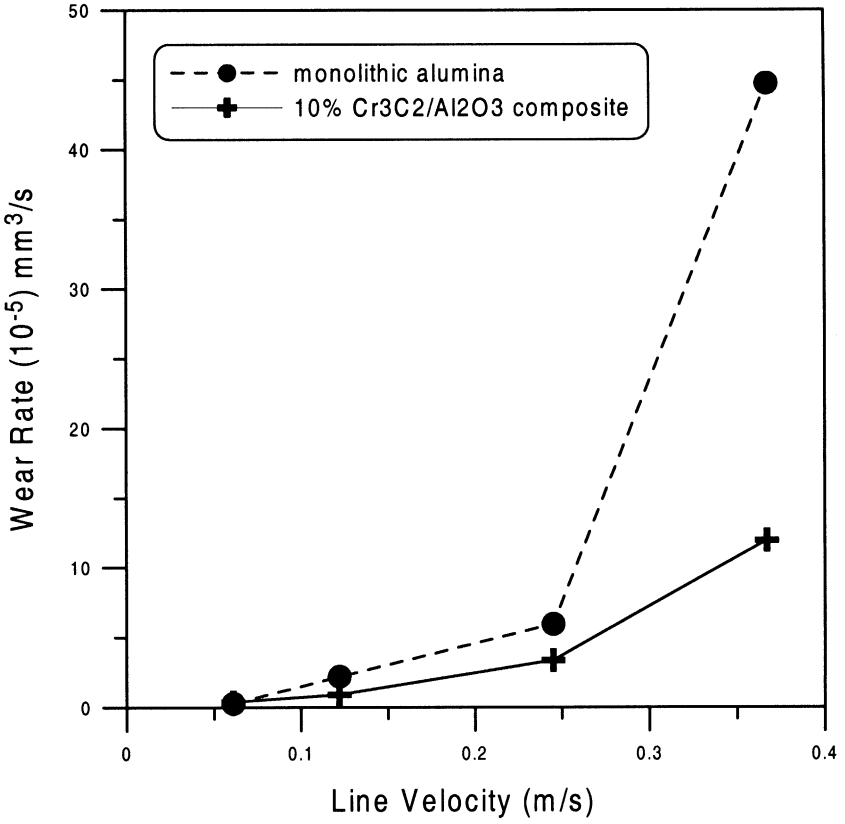

Fig. 3. Volumetric wear rate versus line velocity at 98 N.

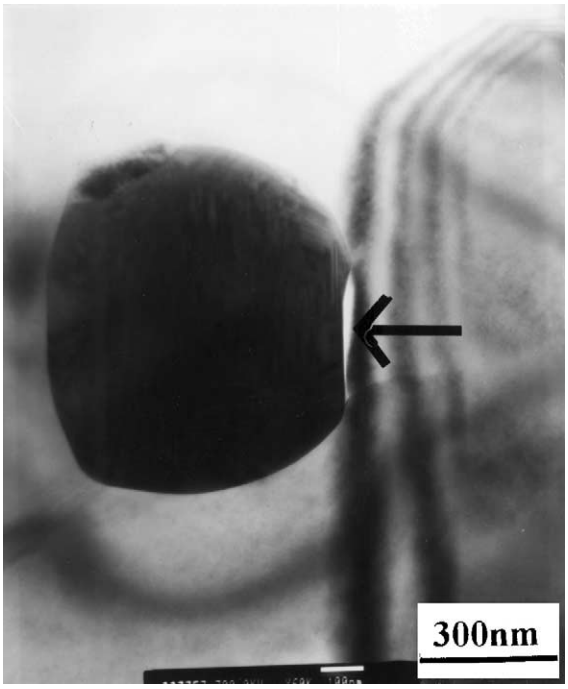

Fig. 4. Microcrack formed by thermal mismatch between the Al_2O_3 matrix and Cr_3C_2 particle. The arrow indicates the microcracking.

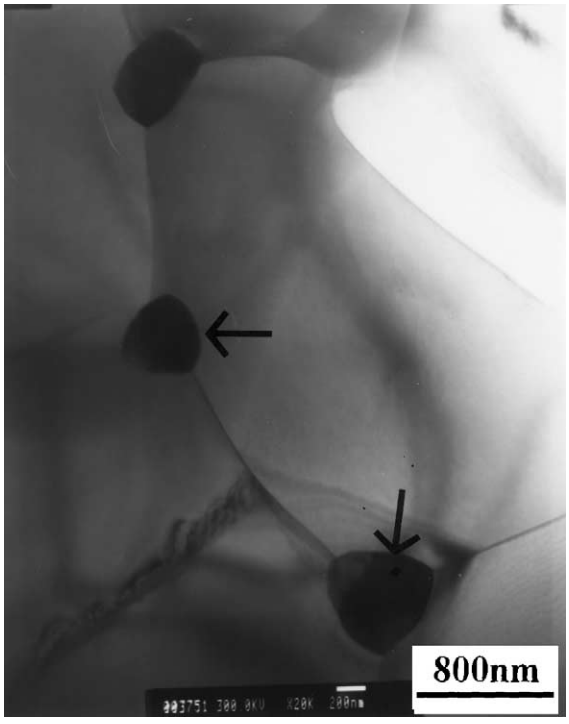

Fig. 5. TEM micrograph of as sintered 10 vol.% Cr_3C_2/Al_2O_3 composite indicating Cr_3C_2 particles located at triple junctions.

where Ψ is a constant ranging from 10 to 70, γ_f is the fracture energy, E_m is the Young's modulus of the matrix, $\Delta\alpha$ is the thermal expansion mismatch and ΔT is the temperature difference over which the mismatch strains build up. **d** was estimated for the Cr_3C_2/Al_2O_3 composite. The used parameters and the results are listed in Table 2. The estimated critical value of grain calculated from Eq. (2) is about 2.2 μm, which is in good agreement with the observations of particle size (3–4 μm) shown in Table 1.

The thermal residual stress in Cr_3C_2/Al_2O_3 composites was theoretically calculated in order to elucidate microcracking. Assuming that the Cr_3C_2 particle is quasi-spherical, the residual stress resulting from differential thermal expansion between the particle and the matrix is given as [21].

$$\sigma_r = -2\sigma_t = -\{((\alpha_m - \alpha_p)\Delta T)\}/[((1+\mu_m)/2E_m) + ((1-2\upsilon_p)/2E_p)]\}(R/r)^3 \quad (3)$$

for $r \geqq R$

where σ_r is the radial stress, σ_t is the tangential stress, α is the thermal expansion coefficient, E is the Young's modulus, ν is the Poisson ratio, subscripts m and p refer to the matrix and particle, respectively, ΔT is the temperature difference, R is the radius of particle and r is the radial distance in the matrix from the center of the particle. The estimated local radial stress at the interface is about 1.0–1.3 GPa (tensile) for $\Delta T = 1500$ °C which is higher than the fracture strength of the composites (490 MPa). A compressive residual stress acting on the matrix in the hoop direction will exceed 500 MPa. Microcracks will be formed depending on the magnitude of stresses.

A typical TEM micrograph of Cr_3C_2/Al_2O_3 composite given in Fig. 5 shows Cr_3C_2 particles situated at triple junctions of alumina particles. Evans and Fu [22,23] computed the stresses along the grain boundaries due to thermal expansion anisotropy for several simple arrays of elastically isotropic hexagonal grains embedded in an infinite matrix. They stated that triple-grain junctions exhibit a logarithmic stress singularity, which gives rise to microcrack initiation. Tvergaard and Hutchinson [24] extended the analyses of grain arrays to include the influence of elastic anisotropy on the stress singularities at triple junctions. Predictions of microcrack initiation in these analyses were made assuming the pre-existence of a grain boundary defect.

Table 2
The parameters and calculated value of **d** (critical particle size) in 10% Cr_3C_2/Al_2O_3 composite

	$\Delta\alpha$ (10^{-6}/°C)	ΔT (°C)	E (GPa)	γ (J/m^2)	**d** (μm)
Cr_3C_2/Al_2O_3	2.4	1500	360	1	2.2

Up to now, there is no theoretical model predicting the correlation between the crack density and critical particle size. More recently, Zimmermann and co-workers [25] tried to provide a simple representation of the simulated cumulative damage distribution for the rising microcrack density as a function of misfit strain.

Previous studies observed no apparent interfacial reaction between Cr_3C_2 and Al_2O_3 using high resolution TEM [26]. The addition of 10% Cr_3C_2 to alumina matrix results in a 20% increase in the fracture toughness. Yet, the wear resistance either remains unchanged or is upgraded slightly. One possible explanation is microcracking in the microstructures.

3.2. Wear mechanisms under ambient conditions

A typical micrograph of a damaged surface of the composite after wear test with a sliding speed of 0.245 m/s and 196 N load is shown in Fig. 6(a). Wear tracks were observed and scratched damage was identified, suggesting that the sliding wear proceeded along with the local fracture and abrasive grooves. The SEM photomicrograph in Fig. 6(b), at a higher magnification, shows cracks parallel to one another and perpendicular to the sliding direction. The straight sliding scratches indicate microplastic deformation.

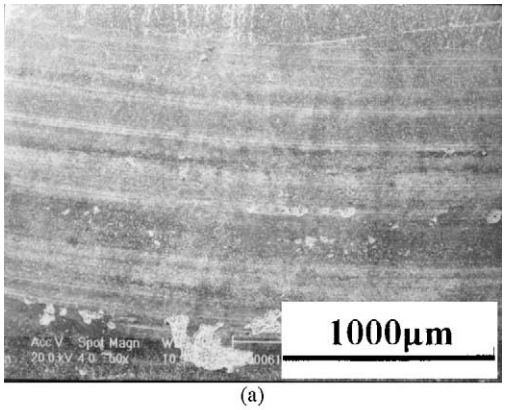

(a)

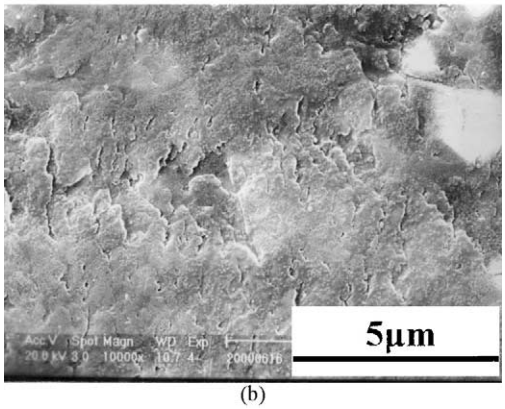

(b)

Fig. 6. SEM micrographs of wear track on 10 vol.% Cr_3C_2/Al_2O_3 composite at 196 N and 0.245 m/s velocity: (a) 50× and (b) 10 000×.

Pullouts of some grains on the worn surface were observed in Fig. 7 suggesting the weak interphase boundaries due to microcracks. Wear debris was collected using a collective tape after 1 km run under the same experimental conditions (196 N and 0.245 m/s) and examined SEM, as shown in Fig. 8. The flake-shaped debris generated were partly recycled through the contact interface during wearing. Some particles of submicrometer size were observed. No changes were detected in the chemical composition and phase transformation of wear debris and worn tracks from results of EDS and ESCA.

3.3. Wear surface residual stress

The residual stress in the wear surface of the 10% Cr_3C_2/Al_2O_3 composite was measured by a $\sin^2\psi$ X-ray diffraction technique, especially focusing on the near-surface region [13,14]. In this study, the (416) lattice plane of Al_2O_3 phase was chosen in the measurement

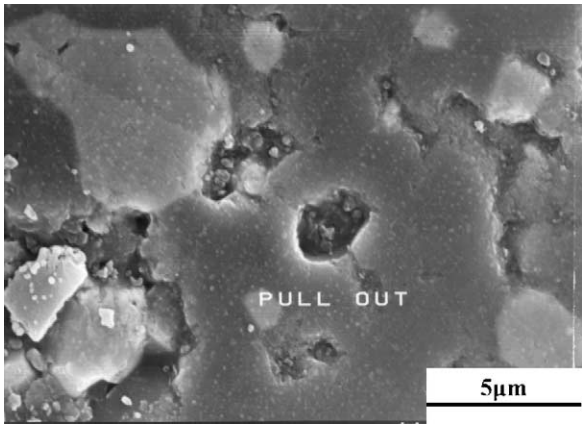

Fig. 7. SEM micrograph showing the grain pull-out on wear track of 10 vol.% Cr_3C_2/Al_2O_3 composite.

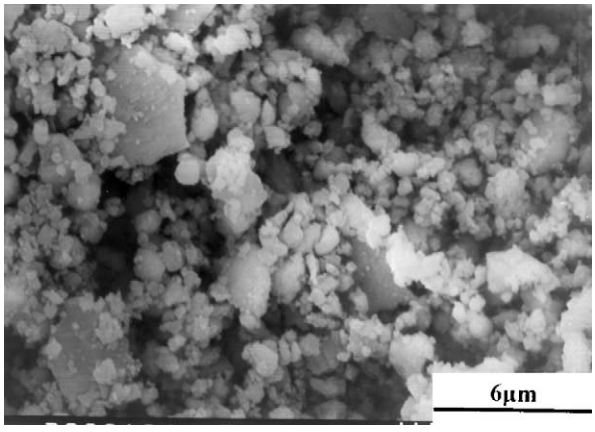

Fig. 8. SEM micrograph of wear debris showing flake shape and grain chipping on wear track of 10 vol.% Cr_3C_2/Al_2O_3 composite.

because of its strong intensity and high diffraction angle. The stress was calculated using the $\sin^2\psi$ method [14]. A residual compressive stress of −59 MPa in as sintered specimen, −142 MPa in worn track samples and −152 MPa in the ground samples were obtained.

The processing-induced microcracking also generates compressive residual stresses. The presence of a surface residual stress was normally resulted from local plastic deformation as well as from microcracking. The difference between as sintered and worn surface samples was likely the result of fracture and grain deformation induced by subsurface sliding wear contact. The role of plasticity in the wear of ceramics is still controversial and little direct experimental verification is available. In general, at high temperature, the main plastic deformation in single crystal alumina is plastic slip by dislocation glide. In polycrystalline alumina, diffusion-driven grain boundary sliding may be an important deformation mechanism [27]. The observed residual stresses provided evidence that micro-plastic deformation occurs during the room-temperature sliding of 10% Cr_3C_2/Al_2O_3 composites even though microplasticity is extremely limited in fine grained microstructures. Plastic flow by dislocation slip has been reported at relatively low temperature (200 °C) in the presence of a confining hydrostatic pressure [28]. However, at room temperature, twinning, possibly compounded by dislocation motion, is always accommodated in either polycrystalline alumina or single crystal sapphire [28].

Several deformation modes were identified, including basal slip, pyramidal slip and basal and rhombohedral twinning [28,29]. Hockey found a dominance of basal slip when indenting alumina in air at room temperature. However, prismatic slip was observed in bulk compression studies below 600 °C by other researchers [29]. This indicates that the surface and environmental effects control significantly surface plasticity. In fact, the no. 270 diamond ground deformed layers contain dislocations, microcracks and plastic deformation. The squeeze grinding process could heat the surface to above 1000 °C, and decreases rapidly below the surface. Both the worn track samples as well as the diamond ground samples get almost the same surface residual stress.

The TEM micrograph shown in Fig. 9 illustrates the dislocation pile up at a subgrain perpendicular to grain boundary. The possible influence of microplasticity in the nucleation of microcrack can be treated in terms of the Zener–Stroh formalism [30,31].

The critical value of the resolved shear stress on an operable slip plane from which a crack will nucleate is expressed by

$$\tau_{\text{crack}} = \left\{[\pi\gamma G f(\Phi)]/[2(1-\mu)d]\right\}^{1/2} \quad (4)$$

where γ is the surface energy associated with the crack; G is the shear modulus; f is a geometrical function of Φ,

Fig. 9. TEM micrograph of as sintered 10 vol.% Cr_3C_2/Al_2O_3 composite showing dislocations pile-up at subgrain.

the angle subtended by the slip plane and the projected crack shown in Fig. 10, ν is the Poisson's ratio and d is the dislocation pileup length related to the characteristic size of the grain. Therefore, as seen in Fig. 10, a variety of crack types may be nucleated, γ can represent either the surface energy for preferential intracrystalline cleavage (1,2), the gain boundary surface energy (3), or the surface energy associated with slip plane cleavage (4) and Cr_3C_2 at triple junction (5). Which mode of cracking is observed in a given case depends on the combination of slip band, grain boundary (triple junctions) and potential cleavage plane orientations.

In addition to sliding contact load, it is important to note that the temperature involved will lead to plastic deformation. Estimation of the flash temperatures induced at the wear track surface by the friction force is difficult, because they are localized and temperature transients occur over a short time. The estimated flash temperature (300–400 °C) is below grounding temperature, but it might also give rise to thermal stress and cracking.

4. Conclusion

1. Spontaneous microcracking during cooling process of sintering was observed and conformed with an estimated critical particle size in 10% Cr_3C_2 /Al_2O_3 composite.

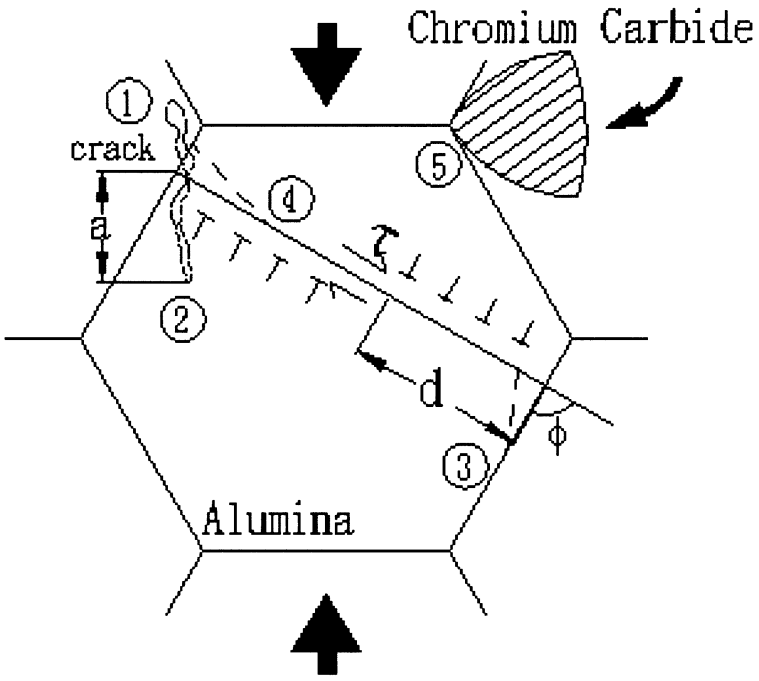

Fig. 10. Geometry of compressive slip band-nucleated intracrystalline cleavage (1, 2), intergranular separation (3), slip band microfracture (4) and chromium carbide at triple junction (5).

2. The addition of Cr_3C_2 to Al_2O_3 matrix improved its macroscopic fracture toughness, but it enhanced its wear resistance only slightly. This suggests that the microcracking induced from residual stresses states could play an important role in predicting its wear behaviors. Particle pullout, wear debris and matrix chipping were observed.
3. The worn surface shows a microabrasive and microplastic deformation. The worn induced surface residual stress (−142 MPa) is close to the surface residual stress induced by no. 270 diamond wheel grinding (−158 MPa).

Acknowledgements

The authors would like to thank the National Science Council, Republic of China, for its support under Grant No. NSC 87-2216-E006-041.

References

[1] C.T. Fu, J.M. Wu, A.K. Li, Microstructure and mechanical properties of Cr_3C_2 particulate reinforced Al_2O_3 matrix composites, J. Mater. Sci. 29 (1994) 2671–2677.
[2] C.T. Fu, A.K. Li, J.M. Wu, Effects of oxidation of Cr_3C_2 particle reinforced Cr_3C_2 matrix composites on microstructure and mechanical structure properties, J. Mater. Sci. 28 (1993) 6285–6294.
[3] C.T. Fu, A.K. Li, J.M. Wu, Effects of post-sinter hot isostatic pressing processes on microstructures and mechanical properties of Al_2O_3-Cr_3C_2 composites, Br. Ceram. Trans. 93 (1994) 178–183.
[4] D.F. Lii, J.L. Huang, K.C. Twu, A.K. Li, Investigation of Al_2O_3/Cr_3C_2 composites prepared by pressureless sintering (part 1), J. Ceram. Soc. Jpn. 104 (1996) 796–801.
[5] J.L. Huang, K.C. Twu, D.F. Lii, A.K. Li, Investigation of Al_2O_3/Cr_3C_2 composites prepared by pressureless sintering (part 2), Mater. Chem. Phys. 51 (1997) 211–215.
[6] J.L. Huang, J.J. Huang, C.A. Jeng, A.K. Li, Investigation of Al_2O_3/Cr_3C_2 composites prepared by pressureless sintering (part 3), Ceram. Int. 25 (1999) 141–144.
[7] H. Liang, T.E. Fischer, Effect of grain boundary impurities on the mechanical and tribological properties of zirconia surfaces, J. Am. Ceram. Soc. 66 (1993) 325–329.
[8] J.D. Oscar Barceinas-Sanchez, W. Mark Rainforth, Transmission electron microscopy of a 3Y-TZP worn under dry and water-lubricated conditions, J. Am. Ceram. Soc. 82 (1999) 1483–1491.
[9] B. Kerkwijk, L. Winnubst, E.J. Mulder, H Verweij, Processing of homogeneous zirconia-toughened alumina ceramics with high dry-sliding wear resistance, J. Am. Ceram. Soc. 82 (1999) 2087–2093.
[10] C.R. Blanchard, R.A. Page, Effect of silicon carbide whisker and titanium carbide particulate additions on the friction and wear behavior of silicon nitride, J. Am. Ceram. Soc. 73 (1990) 3442–3452.
[11] C.P. Dogan, J.A. Hawk, Influence of whisker toughening and microstructure on the wear behavior of Si_3N_4- and Al_2O_3-matrix composites reinforced with SiC, J. Mater. Sci. 35 (2000) 5793–5807.
[12] O.O. Ajayi, A. Erdemir, R.H. Lee, F.A. Nichols, Sliding wear of silicon-titanium boride ceramic-matrix composite, J. Am. Ceram. Soc. 76 (1993) 511–517.

[13] J.B. Cohen, H. Dolle, M.R. James, Stress Analysis from Powder Diffraction Patterns, NBS Special Publication 567, 1980, pp. 453–477.
[14] I.C. Noyan, J.B. Cohen, Residual Stress, Springer Verlag, New York, 1987.
[15] S. Jahanmir, X. Dong, Mechanism of mild to severe wear transition in alpha-alumina, ASME J. Tribol. 114 (1992) 403–411.
[16] A. Blomberg, M. Olsson, S. Hogmark, Wear mechanism and tribo mapping of Al_2O_3 and SiC in dry sliding, Wear 171 (1994) 77–89.
[17] S.C. Lim, M.F. Ashby, Wear mechanism maps, Acta Metall. 35 (1987) 1–24.
[18] H. Kong, M.F. Ashby, Wear mechanisms in brittle solids, Acta Mater. 40 (1992) 2907–2920.
[19] R.W. Rice, Toughening in ceramic particulate and whisker composites, Ceram. Eng. Sci. Proc. 11 (1990) 667–694.
[20] Y.S. Chou, D.J. Green, Silicon carbide platelet/alumina composites: II, mechanical properties, J. Am. Ceram. Soc. 76 (1995) 1452–1458.
[21] J. Selsing, Internal stresses in ceramics, J. Am. Ceram. Soc. (1961) 419.
[22] A.G. Evans, Microfracture from thermal expansion anisotropy—I. Phase systems, Acta Metall. 26 (1978) 1845–1853.
[23] Y. Fu, A.G. Evans, Some effect of microcracks on the mechanical properties of brittle solids—I, Acta Metall. 33 (1985) 1515–1523.
[24] V. Tvergaard, J.W. Hutchinson, Microcracking in ceramics induced by thermal expansion or elastic anisotropy, J. Am. Ceram. Soc. 71 (1988) 157–166.
[25] A. Zimmermann, W.C. Carter, E.R. Fuller Jr, Damage evolution during microcracking of brittle solids, Acta Metall. 49 (2001) 127–137.
[26] D.F. Lii, J.L. Huang, J.J. Huang, H.H. Lu, The interfacial reaction Cr_3C_2/Al_2O_3 composites, J. Mater. Res. 14 (1999) 817–823.
[27] R.M. Cannon, W.H. Rhodes, A.H. Heuer, Plastic deformation of fine-grained alumina (Al_2O_3) I, interface-controlled diffusional creep, J. Am. Ceram. Soc. 63 (1980) 46–53.
[28] B.J. Inkson, Disloctions and twinning activated by the abrasion of Al_2O_3, Acta Metall. 48 (2000) 1883–1895.
[29] J.D. Snow, A.H. Heuer, Slip system in Al_2O_3, J. Am. Ceram. Soc. 56 (1973) 153–157.
[30] J. Lankford, W.W. Predebon, J.M. Staehler, G. Subhash, B.J. Pletka, C.E. Anderson, The role of plasticity as a limiting factor in the compressive failure of high strength ceramics, Mechanics of Materials 29 (1998) 205–218.
[31] D. Krajcinovic, A. Stojimirovic, Deformation processes in semi-brittle polycrystalline ceramics, J. Fracture 42 (1990) 73–86.